IEEE Access
Multidisciplinary | Rapid Review | Open Access Journal

Received March 15, 2020, accepted March 24, 2020, date of publication April 14, 2020, date of current version May 1, 2020.

Digital Object Identifier 10.1109/ACCESS.2020.2987940

Discrete Model Predictive Control Scheme for an Integrated Gauge-Looper Control System in a Tandem Hot Strip Mill

FANGCHEN YIN
Institute of Manufacturing Engineering, Huaqiao University, Xiamen 361021, China
Fujian Engineering Research Center of Intelligent Manufacturing for Brittle Materials, Fujian 361021, China
e-mail: yfc_ral@163.com

This work was supported in part by the Natural Science Foundation of Fujian province under Grant 2019J01084.

ABSTRACT There exists strong coupling and a complex multivariable relation among the strip gauge, looper angle and strip tension in tandem hot rolling. To improve the gauge precision of the hot strip, the dynamic relationship among these three variables must be determined. In this paper, a new coordinated optimal control scheme based on discrete model predictive control (DMPC) theory was presented for an automatic gauge control and looper control (AGC-LP) integrated system. First, a state-space model of the AGC-LP integrated system was established based on a 1700 mm tandem hot strip mill. Then, to achieve the desired dynamic performance with the AGC-LP integrated system, a performance index function and an optimal control sequence were designed for the DMPC controller. The simulation results showed that the proposed DMPC controller had better robustness and adaptability to modeling uncertainties and external disturbances than a traditional proportional-integral (PI) controller.

INDEX TERMS Tandem hot rolling, AGC-LP integrated system, state-space model, discrete model predictive control.

I. INTRODUCTION

The hot strip rolling process transforms cast steel slabs into thin sheets [1]. Figure 1 shows the typical layout of a hot strip mill facility, which consists of a reheating furnace, a roughing mill, shears, a finishing mill, water coolant headers, and a coiler [2], [3]. Bars with a diameter of approximately 250 mm are heated to approximately 1200°C in the reheating furnace. In the roughing mill, the reheated slabs are reduced to a thickness of 25–50 mm. The resulting sheet is then transported to the finishing mill, where it is further reduced to the final thickness 0.8–20 mm.

Thickness precision is one of the most important quality indexes in hot strip milling, and automatic gauge control (AGC) systems, which adjust the gap to control thickness, are the most effective method for ensuring the thickness precision of hot-rolled strip products [4], [5]. The tension variation in the steel strip is one of the main factors that causes thickness fluctuations during hot strip rolling. The constant tension rolling process is usually maintained by a looper control (LP) system, which adjusts the motor torque to control tension [6]. However, the tension is extremely variable in the actual hot rolling process, so a traditional LP system with proportional-integral (PI) control not have sufficient stability to ensure an invariable tension output. An increasing number of electric rolling screw-down systems are being transformed into hydraulic systems. Moreover, the response speed of AGC systems is increasing rapidly. Hence, the interactions between the AGC system and the LP system cannot be ignored [7], [8].

The cooperative optimization of AGC-LP integrated systems is a research hotspot in the field of hot strip rolling control. Hearns and Grimble [9] studied a controller for an AGC-LP integrated system that uses a multivariable H∞ control strategy to enhance system robustness. Okada *et al.* [10] designed a controller with linear quadratic optimal control for an AGC-LP integrated system, which gives the system excellent control accuracy. A state-dependent Riccati equation technique for AGC-LP integrated systems was proposed by Pittner and Simaan [11]. Their results showed that the proposed technique can effectively deal with a highly complex

The associate editor coordinating the review of this manuscript and approving it for publication was Yilun Shang.

This work is licensed under a Creative Commons Attribution 4.0 License. For more information, see https://creativecommons.org/licenses/by/4.0/

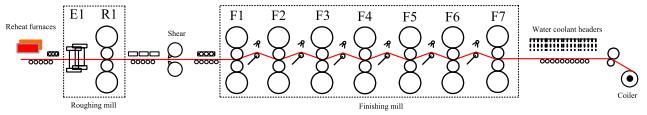

FIGURE 1. Layout of a 1700 mm hot strip mill in a factory.

nonlinear AGC-LP integrated system. Jiao *et al.* [12] developed an adaptive coordinated controller for an AGC-LP integrated system, and the proposed controller was efficient in a wide range of working situations. Qu *et al.* [13] designed a feedback controller with disturbance rejection properties and strong robustness for an AGC-LP integrated system and researched the influence of a multitude of rolling parameters on thickness and tension. Cuzzola [14] developed a multivariable and multiobjective approach for controlling hot strip mills that can explicitly account for actuator limitations and nonlinear dynamics. Hearns and Reeve [15]designed a controller with state feedback and estimation to deal with the unmodeled dynamics of an AGC-LP integrated system. Although the control schemes described above exhibit good performance, they were designed for a continuous model of an AGC-LP system, which makes it difficult to practically apply these control schemes with a programmable logic controller (PLC).

Model predictive control (MPC) theory, which is well known for its simplicity and practicality, has been successfully applied for looper control systems in hot strip finishing mills. For instance, Yin *et al.* [16] introduced dynamic matrix predictive control for hydraulic looper systems, wherein the controller can ensure the system has excellent stability. Choi *et al.* [17] presented a design method for robust MPC, where in the designed controller can simultaneously give the looper system fast response times and strong robustness. To date, no studies have been reported that can verify the robustness and disturbance rejection of the MPC theory for AGC-LP integrated systems. The remaining sections of the paper are organized as follows. In Section 2, a state-space model of an AGC-LP integrated system is established by combining the state equations of an AGC system and an LP system. In Section 3, the proposed control scheme based on discrete model predictive control (DMPC) theory is demonstrated. In Section 4, the control performance of the DMPC control scheme is compared with that of a traditional PI control scheme. The conclusions of the study are presented in Section 5.

II. PROBLEM STATEMENT AND PROCESS MODEL

Figure 2 shows the traditional control system used in hot strip mills, which is mainly composed of an AGC system and an LP system. The LP system is a double closed-loop control system, in which the PI controller and proportional-integral-derivative (PID) controller are designed for the closed-loop control of strip tension and the closed-loop control of the looper angle, respectively. The PI controller adjusts the speed of the downstream stand to control the strip tension, whereas

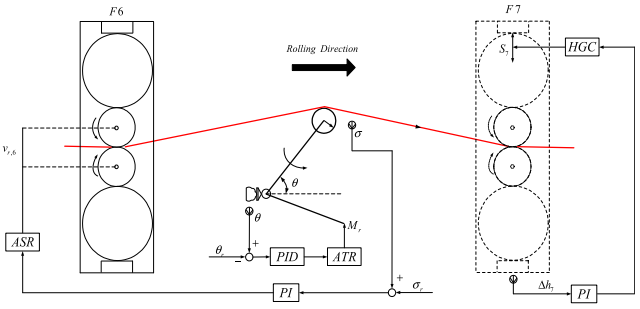

FIGURE 2. Structure of the traditional control system in hot strip mills.

the PID controller adjusts the output torque of the looper motor to control the looper angle. The AGC system contains another PI controller, which adjusts the roll gap to control the strip thickness. The LP system and AGC system run independently in the traditional control system [18].

According to the real characteristics of an AGC system, the high-frequency action of the AGC in the downstream stand is the main disturbance source for the closed-loop control of the strip tension in the LP system. Thus, there is strong coupling among the strip thickness, strip tension and looper angle. In the traditional control system, the above variables can only be controlled in the external system, so the coupling problem cannot be solved. In this paper, the hot rolling process was studied through state-space analysis, and to design a multivariable coordinated controller, an increment equation and a state-space expression for an AGC-LP integrated system were established based on hot rolling theory [19].

A. DYNAMIC DEFORMATION RESISTANCE MODEL

For hot rolling processes, the deformation resistance is an important parameter for establishing a dynamic thickness model and a dynamic tension model. In this paper, the deformation resistance is calculated by the Misaka model [20] as follows:

$$k_f = \begin{cases} 0.28\exp\left(\dfrac{5.0}{T}-\dfrac{0.01}{\rho_C+0.05}\right)\left(\dfrac{\dot{\varepsilon}}{10}\right)^m \\ \quad\times\left[1.3\left(\dfrac{\varepsilon}{0.2}\right)^n-0.3\left(\dfrac{\varepsilon}{0.2}\right)\right], \quad T\geq t_d^0 \\ 0.28g\exp\left(\dfrac{5.0}{T_d}-\dfrac{0.01}{\rho_C+0.05}\right)\left(\dfrac{\dot{\varepsilon}}{10}\right)^m \\ \quad\times\left[1.3\left(\dfrac{\varepsilon}{0.2}\right)^n-0.3\left(\dfrac{\varepsilon}{0.2}\right)\right], \quad T<t_d^0 \end{cases} \tag{1}$$

$$g = 30.0(\rho_C+0.90)\left\{T-0.95\frac{\rho_C+0.49}{\rho_C+0.42}\right\}^2+\frac{\rho_C+0.06}{\rho_C+0.09} \tag{2}$$

$$m = \begin{cases} (-0.019\rho_C+0.126)\,T \\ \quad+(0.075\rho_C+0.050), \quad T\geq t_d^o \\ (0.081\rho_C-0.154)\,T+(-0.019\rho_C+0.207) \\ \quad+\dfrac{0.027}{\rho_C+0.320}, \quad T<t_d^o \end{cases} \tag{3}$$

$$n = 0.41-0.07\rho_C \tag{4}$$

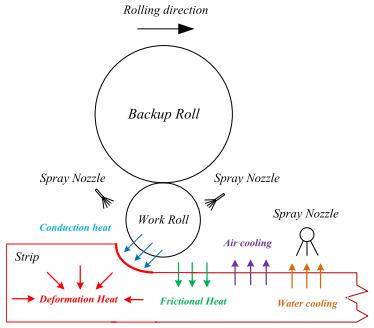

FIGURE 3. Heat flows during hot rolling.

$$\dot{\varepsilon} = \frac{\omega}{60}\sqrt{\frac{R'}{H-h}}\ln\frac{H}{h} \tag{5}$$

By assuming that the carbon content of the strip ρ_C is constant and the deformation resistance k_f is related to the entry thickness H, exit thickness h, the roll rotation speed ω and the rolled workpiece temperature T, the deformation resistance increment model at the ith stand can be obtained as follows:

$$\Delta k_{f,i} = \gamma_{1i}\Delta T_i + \gamma_{2i}\Delta\omega_i + \gamma_{3i}\Delta H_i + \gamma_{4i}\Delta h_i \tag{6}$$

where

$$\gamma_{1i} = \frac{\partial k_{f,i}}{\partial T_i}, \quad \gamma_{2i} = \frac{\partial k_{f,i}}{\partial \omega_i}, \quad \gamma_{3i} = \frac{\partial k_{f,i}}{\partial h_{\text{in},i}}, \quad \gamma_{4i} = \frac{\partial k_{f,i}}{\partial h_{\text{out},i}}$$

As shown in Eqs. (1)-(5), the phase transition temperature is used as the cutoff point, and the different mathematical models were established above and below the phase transition temperature in the Misaka model. Thus, a temperature prediction model for the hot rolling process must be established to calculate the deformation resistance. The temperature prediction model can be divided into two parts: (1) a model for heat dissipation of adjacent stands, which contains an air cooling model and a water cooling model, and (2) a model for heat transfer in the deformation zone, which contains a model of deformation heat, a model of heat conduction, and a model of frictional heat. Figure 3 shows the heat flows during hot rolling [21], [22].

1) AIR COOLING

The heat transferred between the metal and the air is mainly in the form of radiation, but some heat is also transferred to the air by convection cooling. However, convection only accounts for 5-7% of the overall temperature drop caused by air cooling, which is approximately 1000°C. Hence, only the radiation is considered when establishing the model of air cooling, and the other factors are contained in the thermal emittance ε_s, which can be calculated based on the measured data. The air cooling model is established as follows:

$$\Delta T_a = \left[(T+273)^{-3} + \frac{6\varepsilon_s\sigma_s l}{\rho C\omega R}\left(\frac{1}{W}+\frac{1}{l}+\frac{1}{h_{\text{out}}}\right)\right]^{-1/3} - (T+273) \tag{7}$$

2) WATER COOLING

The temperature drop caused by water cooling contains the high-pressure water descaling and interstand cooling, and these two parts are established based on the same mathematical model as follows [20]:

$$\Delta T_{\text{W}} = k_{\text{T}} \cdot \frac{(T - T_{\text{w}}) \cdot f_{\text{s}} \cdot p}{h\nu\rho C} \tag{8}$$

3) DEFORMATION HEAT

The plastic deformation of the workpiece results in work hardening, and the accumulated mechanical energy in work-hardened structures will be released in the form of heat, which increases the strip temperature. The deformation heat model is expressed as follows:

$$\Delta T_{\text{d}} = \frac{p_c\eta}{Wl_{\text{c}}\rho C}\ln\frac{H}{h} \tag{9}$$

4) FRICTIONAL HEAT

Frictional heat comes from the relative sliding between the interface of the roll and the scale layer, and the frictional heat is absorbed by the strip, which increases the temperature of the strip. The frictional heat model can be expressed as follows:

$$\Delta T_f = k_{\text{d}}\frac{1000p_c}{Wl_{\text{c}}C\rho} \tag{10}$$

where k_{d} is the coefficient of friction.

Based on the models established above, the temperature change in the strip ΔT when the strip travels from the ith stand to the i+1th stand can be predicted as follows:

$$\Delta T = \Delta T_f + \Delta T_{\text{d}} - \Delta T_{\text{a}} - \Delta T_{\text{w}} \tag{11}$$

B. DYNAMIC THICKNESS MODEL

In the hot rolling process, the exit thickness of the strip can be calculated from the predicted rolling force, which is estimated with the Sims rolling force model. The rolling force per unit width that is exerted on the rolls by the deforming metal sheet is obtained as follows:

$$F = Q_P\sqrt{R'(H-h)}\left(1.15k_f - m_f\sigma_f - m_b\sigma_b\right) \tag{12}$$

$$R' = R\left[1 + \frac{16(1-\nu^2)F}{\pi E(H-h)}\right] \tag{13}$$

Note that Q_{p} is a geometrical factor developed by Ford and Alexander [23], which is expressed as follows:

$$Q_{\text{P}} = 0.786 + \frac{\sqrt{1-\varepsilon}}{2\sqrt{2\,(2-\varepsilon)}}\frac{\sqrt{R'h(H-h)}}{h} \tag{14}$$

where $\varepsilon = \frac{H-h}{h}$.

By assuming that the initial roll radius is constant, the rolling force increment model at the ith stand ΔF_i can be obtained as follows:

$$\Delta F_i = \alpha_{1i}\Delta H_i + a_{2i}\Delta h_i + \alpha_{3i}\Delta\sigma_{\text{f},i} + \alpha_{4i}\Delta\sigma_{\text{b},i} + \alpha_{5i}\Delta k_{f,i} \tag{15}$$

where

$$\alpha_{1i} = \frac{\partial F_i}{\partial H_i}, \quad \alpha_{2i} = \frac{\partial F_i}{\partial h_i}, \quad \alpha_{3i} = \frac{\partial F_i}{\partial \sigma_{\mathrm{f},i}},$$
$$\alpha_{4i} = \frac{\partial F_i}{\partial \sigma_{\mathrm{b},i}}, \quad \alpha_{5i} = \frac{\partial F_i}{\partial k_{f,i}}$$

The exit strip thickness can be calculated by the roll gap without load and the rolling mill spring deformation under the rolling force, which is called the spring formula. This formula is expressed as follows:

$$h = S_0 + \frac{F - F_0}{M_{\mathrm{m}}} \tag{16}$$

The increment in the spring formula at the ith stand can be obtained as follows:

$$\Delta h_i = \Delta S_i + \frac{\Delta F_i}{M_{\mathrm{m},i}} \tag{17}$$

Therefore, according to Eq. (6), Eq. (15) and Eq. (17), the dynamic thickness increment model can be expressed as follows:

$$\Delta h_i = a_{S,i}\Delta S_i + a_{h_i}\Delta h_i + a_{\sigma_{\mathrm{f},i}}\Delta\sigma_{\mathrm{f},i} + a_{\sigma_{\mathrm{b},i}}\Delta\sigma_{\mathrm{b},i} + a_{T,i}\Delta T_i + a_{\omega,i}\Delta\omega_i \tag{18}$$

where

$$a_{S,i} = \frac{M_{\mathrm{m},i}}{M_{\mathrm{m},i} - \alpha_{2i} - \alpha_{5i}\gamma_{4i}}, \quad a_{h_{\mathrm{in},i}} = \frac{\alpha_{1i} + \alpha_{5i}\gamma_{3i}}{M_{\mathrm{m,i}} - \alpha_{2i} - \alpha_{5i}\gamma_{4i}},$$
$$a_{\sigma_{\mathrm{in},i}} = \frac{\alpha_{3i}}{M_{\mathrm{m},i} - \alpha_{2i} - \alpha_{5i}\gamma_{4i}},$$
$$a_{\sigma_{\mathrm{out},i}} = \frac{\alpha_{4i}}{M_{\mathrm{m},i} - \alpha_{2i} - \alpha_{5i}\gamma_{4i}}, \quad a_{T,i} = \frac{\alpha_{5i}\gamma_{1i}}{M_{\mathrm{m},i} - \alpha_{2i} - \alpha_{5i}\gamma_{4i}},$$
$$a_{\omega,i} = \frac{\alpha_{5i}\gamma_{2i}}{M_{\mathrm{m},i} - \alpha_{2i} - \alpha_{5i}\gamma_{4i}}$$

C. DYNAMIC STRIP TENSION AND LOOPER ANGLE MODELS

1) DYNAMIC STRIP TENSION MODEL

In the actual rolling process, the length of the strip between stands is always longer than the actual length of the strip, and the interstand strip tension $\sigma\ (t)$ can be calculated by the Young's modulus and elongation of the strip according to the following equation:

$$\sigma\ (t) = \frac{E\left[L\ (\theta) - (L + \delta_v\ (t))\right]}{L + \delta_v\ (t)} \tag{19}$$

where $\delta_v\ (t)$ is the mass flow difference in the strip between stands, which can be evaluated as follows:

$$\Delta\delta_{\mathrm{v}}\ (t) = \int_0^t \left[\Delta v_{\mathrm{in,i+1}}\ (t) - \Delta v_{\mathrm{out,i}}\ (t)\right] dt \tag{20}$$

In the actual product, the working roller speed is not equal to the strip speed because forward slip or backward slip occurs between the strip surface and the working roller surface. The forward slip at the ith stand f_{i} and the backward slip at the ith stand b_{i} can be defined as follows:

$$f_i = \frac{v_{\mathrm{out},i} - V_i}{V_i} \times 100\% \tag{21}$$

$$b_i = \frac{V_i - v_{\mathrm{in},i}}{V_i} \times 100\% \tag{22}$$

Based on the mass flow balancing principle, Eqs. (21) and (22) can be rewritten as follows:

$$H_i(1 - b_i) = h_i(1 + f_i) \tag{23}$$

$$b_i = 1 - \frac{h_i}{H_i}(1 + f_i) \tag{24}$$

According to Eq. (21), Eq. (22) and Eq. (24), the increment models of $v_{\mathrm{out},i}$, $v_{\mathrm{in},i+1}$ and b_{i} can be expressed as follows:

$$\Delta v_{out,i} = \Delta V_i(1 + f_i) + \Delta f_i V_i \tag{25}$$

$$\Delta v_{in,i+1} = \Delta V_{i+1}(1 - b_{i+1}) - \Delta b_{i+1} V_{i+1} \tag{26}$$

$$\Delta b_i = -\frac{h_{\mathrm{out},i}}{h_{\mathrm{in},i}}\Delta f_i - \frac{1 + f_i}{h_{\mathrm{in},i}}\Delta h_{\mathrm{out},i} + \frac{(1 + f_i)h_{\mathrm{out},i}}{h_{\mathrm{in},i}^2}\Delta h_{\mathrm{in},i} \tag{27}$$

The slip is a difference between the working roller circumferential speed and the strip speed, which is evaluated by the forward slip equation derived by Sims in this study [24].

$$f = \frac{R'}{h}\phi_n^2 \tag{28}$$

$$\phi_n = \sqrt{\frac{h}{R'}}\tan\left[\frac{1}{2}\arctan\sqrt{\frac{\varepsilon}{1 - \varepsilon}} + \frac{\pi}{8}\ln(1 - \varepsilon) \times \sqrt{\frac{h}{R'}} + \frac{1}{2}\sqrt{\frac{h}{R'}}\frac{\sigma_{\mathrm{f}} - \sigma_{\mathrm{b}}}{k_f}\right] \tag{29}$$

According to Eq. (28) and Eq. (29), the forward slip increment model at the ith stand can be obtained as follows:

$$\Delta f_i = \beta_{1i}\Delta H_i + \beta_{2i}\Delta h_i + \beta_{3i}\Delta\sigma_{\mathrm{f},i} + \beta_{4\mathrm{i}}\Delta\sigma_{\mathrm{b},i} + \beta_{5i}\Delta k_{f,i} \tag{30}$$

where

$$\beta_{1i} = \frac{\partial f_i}{\partial H_i}, \beta_{2i} = \frac{\partial f_i}{\partial h_i}, \beta_{3i} = \frac{\partial f_i}{\partial \sigma_{\mathrm{f},i}}, \beta_{4i} = \frac{\partial f_i}{\partial \sigma_{\mathrm{b},i}}, \beta_{5i} = \frac{\partial f_i}{\partial k_{f,i}}$$

Based on Eq. (19), the interstand tension increment model between the ith stand and the i+1th stand can be obtained as follows:

$$\Delta\dot{\sigma}_{\mathrm{out},i} = \frac{E}{L}\left[\Delta\dot{L}(\theta) + (\Delta v_{\mathrm{in},i+1} - \Delta v_{\mathrm{out},i})\right] \tag{31}$$

By substituting Eq. (25), Eq. (26), Eq. (27) and Eq. (30) into Eq. (31), the dynamic model of strip tension can be expressed as follows:

$$\begin{aligned}\Delta\dot{\sigma}_{out,i} = \frac{E}{L}(&b_{\sigma_{\mathrm{in},i}}\Delta\sigma_{\mathrm{in},i} + b_{\sigma_{out,i+1}}\Delta\sigma_{out,i+1} + b_{\sigma_{out,i}}\Delta\sigma_{out,i} \\ &+ b_{T_i}\Delta T_i + b_{T_{i+1}}\Delta T_{i+1} + b_{H_{i+1}}\Delta H_{i+1} \\ &+ b_{h_{\mathrm{in},i}}\Delta H_i + b_{S_i}\Delta S_i + b_{S_{i+1}}\Delta S_{i+1} \\ &+ b_{\omega_{i+1}}\Delta\omega_{i+1} + b_{\omega_i}\Delta\omega_i + b_{\omega_{L,i}}\Delta\omega_{L,i})\end{aligned} \tag{32}$$

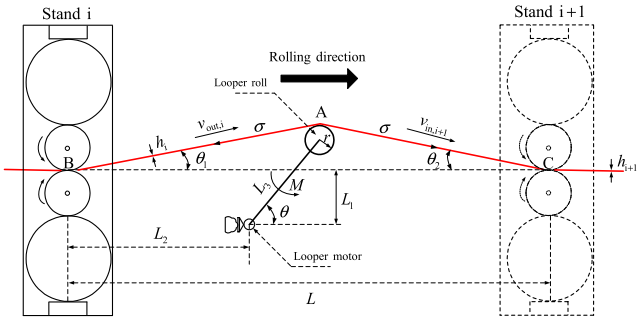

FIGURE 4. A schematic drawing of the looper system.

2) DYNAMIC LOOPER ANGLE MODEL

Figure 4 shows a simplified schematic drawing of the looper system.

The looper angle θ is determined as follows:

$$\frac{d\theta}{dt} = \omega, \quad \theta(0) = \theta_0 \tag{33}$$

where ω is the looper angular velocity, which is derived from Newton's second law of motion. This velocity term can be described as follows:

$$\frac{d\omega}{dt} = \frac{1}{J}\left(M - M_{\mathrm{L}} - M_{\mathrm{g}} - c_{\mathrm{f}}\omega\right) \tag{34}$$

$$M_{\mathrm{L}} = F_{\mathrm{T}} L_3 \tag{35}$$

$$M_g = (W_R g + 0.5 W_S g) L_3 \cos\theta \tag{36}$$

where F_{T} is the tangential force act on the looper roll. This tangential force can be expressed as follows:

$$F_{\mathrm{T}} = F_{\mathrm{tT}} + F_{\mathrm{bfgT}} + F_{\mathrm{s,cfT}} + F_{\mathrm{s,ifT}} + F_{\mathrm{l,ifT}} \tag{37}$$

where F_{tT}, F_{bfgT}, $F_{\mathrm{s,cfT}}$, $F_{\mathrm{s,ifT}}$, and $F_{\mathrm{l,ifT}}$ are the interstand tension, strip bending force and weight, strip centrifugal force, strip inertia force and looper roll inertia force, respectively. These terms can be expressed as follows:

$$F_{\mathrm{tT}} = \sigma W h[\sin(\theta + \theta_2) - \sin(\theta - \theta_1)] \tag{38}$$

$$F_{\mathrm{bfgT}} = \left[16E \cdot W \cdot (L_3 \sin\theta - L_1 + r) \cdot (\frac{h}{L})^3 + \frac{1}{2} W_{\mathrm{S}} \cdot g + W_{\mathrm{R}} \cdot g\right] \cos\theta \tag{39}$$

$$F_{\mathrm{s,cfT}} = -(\theta_1 + \theta_2) \cdot W \cdot h \cdot \rho \cdot \omega^2 \cdot \cos\theta \tag{40}$$

$$F_{\mathrm{s,ifT}} = 0.25 W_{\mathrm{S}} L_3 \ddot{\theta} [\cos(\theta - \theta_1)]^2 + 0.25 W_{\mathrm{S}} L_3 \ddot{\theta} [\cos(\theta + \theta_2)]^2 \tag{41}$$

$$F_{\mathrm{l,ifT}} = W_{\mathrm{R}} \cdot L_3 \times \ddot{\theta} \tag{42}$$

By substituting Eqs. (38)-(42) into Eq. (34), the dynamic looper angle model can be obtained as follows:

According to Eq. (43), as shown at the bottom of this page, the dynamic looper angle increment model at the ith stand can be expressed as follows:

$$\Delta\ddot{\theta}_i = \frac{\partial f_{\mathrm{lp},i}}{\partial \theta_i}\Delta\theta_i + \frac{\partial f_{\mathrm{lp},i}}{\partial M_i}\Delta M_i + \frac{\partial f_{\mathrm{lp},i}}{\partial \sigma_{\mathrm{out},i}}\Delta\sigma_{out,i} + \frac{\partial f_{\mathrm{lp},i}}{\partial \omega_{L,i}}\Delta\omega_{L,i} \tag{44}$$

D. STATE-SPACE MODEL

In the AGC-LP integrated system, the automatic speed regulator (ASR), the automatic torque regulator (ATR) and the hydraulic gap control (HGC) system of stand i are all modeled as a first-order system as follows [24]:

$$\dot{S}_i(t) = \frac{S_{ref,i}(t) - S_i(t)}{\tau_{S,i}}, \quad S_i(0) = S_0 \tag{45}$$

$$\dot{V}_i(t) = \frac{V_{ref,i}(t) - V_i(t)}{\tau_{V,i}}, \quad V_i(0) = V_0 \tag{46}$$

$$\dot{M}_i(t) = \frac{M_{ref,i}(t) - M_i(t)}{\tau_{M,i}}, \quad M(0) = M_0 \tag{47}$$

where $S_{\mathrm{ref}}(t)$, $v_{\mathrm{ref}}(t)$ and $M_{\mathrm{ref}}(t)$ are the control input references of $S(t)$ in the HGC system, $v(t)$ in the ASR and $M(t)$ in the ATR, respectively; and τ_S, τ_{v} and τ_{M} are the time constants of the HGC system, ASR and ATR, respectively.

There is a certain amount of delay in the thickness change as the strip transfers between stands, and this delay can be calculated as follows:

$$\tau_{\mathrm{d},i,i+1} = \frac{L}{\omega_{\mathrm{r},i} R_i (1 + f_i)} \tag{48}$$

The transport delay for the strip thickness can be expressed as first-order lag:

$$\Delta H_{i+1} = \frac{1}{1 + \tau_{\mathrm{d},i,i+1} s}\Delta h_i \tag{49}$$

The temperature is not constant throughout the same strip: the temperature along the length direction of the strip increases due to the change in strain rate induced by increases in the rolling speed. The variation rate for the temperature delay can be calculated as follows:

$$\Delta T_{i+1} = \frac{1}{1 + \tau_{\mathrm{d},i,i+1} s}\left(\Delta T_i + \psi_{1i}\Delta\omega_i + \psi_{2i}\Delta T_{0,i}\right) \tag{50}$$

$$\begin{aligned}\ddot{\theta} &= f_{\mathrm{lp}}(M, \theta, \sigma) \\ &= \frac{M - L_3 w h \sigma[\sin(\theta + \theta_2) - \sin(\theta - \theta_1)] - L_3 \cos\theta\left[16E \cdot w \cdot (L_3 \sin\theta - L_1 + r) \cdot (\frac{h}{L})^3 + \frac{1}{2} W_{\mathrm{S}} \cdot g + W_{\mathrm{R}} \cdot g\right]}{0.25 L_3^2 W_{\mathrm{S}}\left\{[\cos(\theta - \theta_1)]^2 + [\cos(\theta + \theta_2)]^2\right\} + J + W_{\mathrm{R}}(L_3)^2} \\ &\quad - \frac{(\theta_1 + \theta_2) \cdot w \cdot h \cdot \rho \cdot \omega^2 \cdot L_3 \cos\theta + c_{\mathrm{f}}\omega_{\mathrm{L}}}{0.25 L_3^2 W_{\mathrm{S}}\left\{[\cos(\theta - \theta_1)]^2 + [\cos(\theta + \theta_2)]^2\right\} + J + W_{\mathrm{R}}(L_3)^2}\end{aligned} \tag{43}$$

where

$$\psi_{1i} = \frac{\partial T_i}{\partial \omega_i}, \psi_{2i} = \frac{\partial T_i}{\partial T_{0,i}}$$

Based on the increment models of strip thickness, strip tension and looper angle established above, the state-space model focusing on the ith stand and i+1th stand can be expressed as follows:

$$\begin{cases} \dot{\boldsymbol{x}}_i = \boldsymbol{A}_i \boldsymbol{x}_i + \boldsymbol{B}_i \boldsymbol{u}_i + \boldsymbol{D}_{\text{in},i} \boldsymbol{d}_i \\ \boldsymbol{y}_i = \boldsymbol{C}_i \boldsymbol{x}_i + \boldsymbol{D}_{\text{out},i} \boldsymbol{d}_i \end{cases} \tag{51}$$

where $\boldsymbol{x}_i$ is the state vector for the ith stand, $\boldsymbol{u}_\text{i}$ is the control vector for the ith stand, $\boldsymbol{d}_\text{i}$ is the disturbance vector for the ith stand, and $\boldsymbol{y}_\text{i}$ is the output vector for the ith stand.

$$\begin{aligned} \boldsymbol{x}_i &= [\Delta\sigma_{\text{out},i}\ \Delta\theta_i\ \Delta\omega_{L,i}\ \Delta T_{\text{in},i+1}\ \Delta\omega_i\ \Delta\omega_{i+1} \\ &\quad \Delta M_i\ \Delta S_i\ \Delta S_{i+1}]^T \\ \boldsymbol{u}_i &= [\,\Delta\omega_{\text{ref},i}\ \ \Delta\omega_{\text{ref},i+1}\ \ \Delta M_{\text{ref},i}\ \ \Delta S_{\text{ref},i}\ \ \Delta S_{\text{ref},i+1}\,]^T \\ \boldsymbol{d}_i &= [\,\Delta h_i\ \ \ \Delta h_{i+1}\ \ \ \Delta\sigma_{\text{in},i}\ \ \ \Delta\sigma_{\text{out},i+1}\ \ \ \Delta T_{in,i}\,]^T \\ \boldsymbol{y}_i &= [\,\Delta\sigma_{\text{out},i}\ \ \ \Delta\theta_i\ \ \ \Delta H_i\,]^T \end{aligned}$$

The coefficient matrix satisfies the following form: $\boldsymbol{A}_i$, as shown at the bottom of the next page,

To validate the established state-space model of the AGC-LP integrated system, the 6th stand, the 7th stand and the 6th looper of a 1700 mm hot finishing mill are used as control objects. For this validation process, the specification of the rolling strip is 1265 mm×2.5 mm, the required data collected from an actual seven-stand hot mill were input into the model, and the mill exit temperature, exit gauge, looper angle and roll gap were calculated in MATLAB. Figure 5 shows that the predicted exit temperature and looper angle were consistent with the trends of the actual measured data, and the corresponding error was very small. Although the error in the looper angle and roll gap reached 10% and 15%, respectively, the looper angle and roll gap had strong correlations with the actual measured data and the error was within the allowable tolerable range. Therefore, the comparison verified the established state-space model is valid and reasonable.

III. DMPC CONTROLLER DESIGN

A. DMPC DESIGN THEORY

The traditional MPC control theory is only designed for continuous model. However, most of the hot strip mill lines are controlled by PLC, so the discrete model predictive controller designed for discrete model can meet the requirements of practical applications, and the adoption of high-performance PLC makes the DMPC easy to be realized in the system [25]–[27].

In this section, the AGC-LP integrated continuous model is discretized with an actual sampling period. Since the model given in Eq. (50) is not suitable for controller design, a discrete state-space model of the AGC-LP integrated system at stand i was established through state reduction as follows:

$$\begin{cases} \bar{\boldsymbol{x}}_i(k+1) = \bar{\boldsymbol{A}}_i \bar{\boldsymbol{x}}_i(k) + \bar{\boldsymbol{B}}_i \bar{\boldsymbol{u}}_i(k) + \bar{\boldsymbol{D}}_i \bar{\boldsymbol{d}}_i(k) \\ \bar{\boldsymbol{y}}_i(k) = \bar{\boldsymbol{C}}_i \bar{\boldsymbol{x}}_i(k) \end{cases} \tag{52}$$

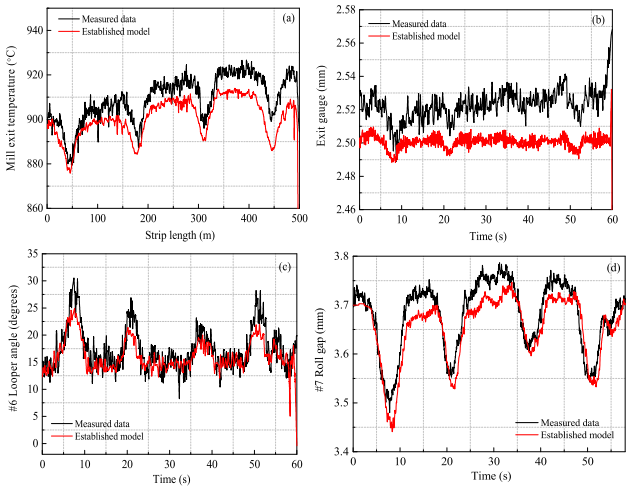

FIGURE 5. Comparison of actual and simulated results: (a) exit temperature, (b) exit gauge, (c) looper angle, and (d) roll gap.

where

$$\begin{aligned} \bar{\boldsymbol{A}}_i &= e^{\boldsymbol{A}_i T} \\ \bar{\boldsymbol{C}}_i &= e^{\boldsymbol{C}_i T} \\ \bar{\boldsymbol{B}}_i &= \left(\int_0^T e^{\boldsymbol{A}_i T} dt\right) \boldsymbol{B}_i \\ \bar{\boldsymbol{D}}_i &= \left(\int_0^T e^{\boldsymbol{A}_i T} dt\right) \boldsymbol{D}_i \\ \bar{\boldsymbol{x}}_i(\mathrm{k}) &= \left[\,\Delta\theta_i\ \ \Delta\omega_{L,i}\ \ \Delta\sigma_{out,i}\ \ \Delta\omega_i\ \ \Delta M_i\ \ \Delta S_{i+1}\,\right]_{kT}^T \\ \bar{\boldsymbol{u}}_i(\mathrm{k}) &= \left[\,\Delta\omega_{r,i}\ \ \ \Delta M_{r,i}\ \ \ \Delta S_{r,i+1}\,\right]_{kT}^T \\ \bar{\boldsymbol{d}}_i(\mathrm{k}) &= \left[\,\Delta h_{in,i}\ \ \ \Delta T_i\ \ \ \Delta T_{i+1}\,\right]_{kT}^T \\ \bar{\boldsymbol{y}}_i(\mathrm{k}) &= \left[\,\Delta\theta_i(t)\ \ \ \Delta\sigma_{out,i}(t)\ \ \ \Delta h_{out,i+1}(t)\right]_{kT}^T \end{aligned}$$

Eq. (52) is converted to an incremental formulation as follows:

$$\Delta\bar{\boldsymbol{x}}_i(k+1) = \bar{\boldsymbol{A}}_i \Delta\bar{\boldsymbol{x}}_i(k) + \bar{\boldsymbol{B}}_i \Delta\bar{\boldsymbol{u}}_i(k) + \bar{\boldsymbol{D}}_i \Delta\bar{\boldsymbol{d}}_i(k) \tag{53}$$

where

$$\begin{aligned} \Delta\bar{\boldsymbol{x}}_i(k+1) &= \bar{\boldsymbol{x}}_i(k+1) - \bar{\boldsymbol{x}}_i(k),\ \ \Delta\bar{\boldsymbol{x}}_i(k) = \bar{\boldsymbol{x}}_i(k) - \bar{\boldsymbol{x}}_i(k-1), \\ \Delta\bar{\boldsymbol{u}}_i(k) &= \bar{\boldsymbol{u}}_i(k) - \bar{\boldsymbol{u}}_i(k-1),\ \ \Delta\bar{\boldsymbol{d}}_i(k) = \bar{\boldsymbol{d}}_i(k) - \bar{\boldsymbol{d}}_i(k-1). \end{aligned}$$

The system output can then be rewritten as follows:

$$\begin{aligned} \Delta\bar{\boldsymbol{y}}_i(k+1) &= \Delta\bar{\boldsymbol{y}}_i(k+1) - \Delta\bar{\boldsymbol{y}}_i(k) \\ &= \bar{\boldsymbol{C}}_i \bar{\boldsymbol{x}}_i(k+1) - \bar{\boldsymbol{C}}_i \bar{\boldsymbol{x}}_i(k) \\ &= \bar{\boldsymbol{C}}_i \Delta\bar{\boldsymbol{x}}_i(k+1) \\ &= \bar{\boldsymbol{C}}_i \bar{\boldsymbol{A}}_i \Delta\bar{\boldsymbol{x}}_i(k) + \bar{\boldsymbol{C}}_i \bar{\boldsymbol{B}}_i \Delta\bar{\boldsymbol{u}}_i(k) + \bar{\boldsymbol{C}}_i \bar{\boldsymbol{D}}_i \Delta\bar{\boldsymbol{d}}_i(k) \end{aligned} \tag{54}$$

$$\begin{aligned} \bar{\boldsymbol{y}}_i(k+1) &= \bar{\boldsymbol{C}}_i \bar{\boldsymbol{A}}_i \Delta\bar{\boldsymbol{x}}_i(k) + \bar{\boldsymbol{C}}_i \bar{\boldsymbol{B}}_i \Delta\bar{\boldsymbol{u}}_i(k) \\ &\quad + \bar{\boldsymbol{C}}_i \bar{\boldsymbol{D}}_i \Delta\bar{\boldsymbol{d}}_i(k) + \bar{\boldsymbol{y}}_i(k) \end{aligned} \tag{55}$$

The new state variable is built as $\boldsymbol{x}_i(k) = [\Delta\bar{\boldsymbol{x}}_i(k) \boldsymbol{y}(k)]^T$, and the AGC-LP integrated system based on the augmented state-

space model can be written as follows:

$$\begin{cases} \begin{bmatrix} \Delta\bar{\boldsymbol{x}}_i(k+1) \\ \boldsymbol{y}_i(k+1) \end{bmatrix} = \begin{bmatrix} \bar{\boldsymbol{A}}^i_{6\times6} & \boldsymbol{O}_{6\times3} \\ \bar{\boldsymbol{C}}^i_{3\times6}\bar{\boldsymbol{A}}^i_{6\times6} & \boldsymbol{I}_{3\times3} \end{bmatrix} \begin{bmatrix} \Delta\bar{\boldsymbol{x}}_i(k) \\ \boldsymbol{y}_i(k) \end{bmatrix} \\ \quad + \begin{bmatrix} \bar{\boldsymbol{B}}^i_{6\times3} \\ \bar{\boldsymbol{C}}^i_{3\times6}\bar{\boldsymbol{B}}^i_{6\times3} \end{bmatrix} \Delta\bar{\boldsymbol{u}}_i(k) + \begin{bmatrix} \bar{\boldsymbol{D}}^i_{6\times3} \\ \bar{\boldsymbol{C}}^i_{3\times6}\bar{\boldsymbol{D}}^i_{6\times3} \end{bmatrix} \Delta\bar{\boldsymbol{d}}_i(k) \\ \boldsymbol{y}_i(k) = \begin{bmatrix} \boldsymbol{O}_{3\times6} & \boldsymbol{I}_{3\times3} \end{bmatrix} \begin{bmatrix} \Delta\bar{\boldsymbol{x}}_i(k) \\ \boldsymbol{y}_i(k) \end{bmatrix} \end{cases} \tag{56}$$

Eq. (56) can be rewritten in a compact form as follows:

$$\begin{cases} \boldsymbol{x}_i(k+1) = \boldsymbol{A}_i\boldsymbol{x}_i(k) + \boldsymbol{B}_i\boldsymbol{u}_i(k) + \boldsymbol{D}_i\boldsymbol{d}_i(k) \\ \boldsymbol{y}_i(k) = \boldsymbol{C}_i\boldsymbol{x}_i(k) \end{cases} \tag{57}$$

At time $k = k_n$, the AGC-LP integrated system starts to move with an initial state $\boldsymbol{x}_i(k_n)$, and the sequences of the control

$$\boldsymbol{A}_i = \begin{bmatrix} \frac{E}{L}b\sigma_{\text{out},i} & 0 & \frac{E}{L}b\omega_{L,i} & \frac{E}{L}bT_{i+1} & \frac{E}{L}b\omega_i & \frac{E}{L}b\omega_{i+1} & 0 & \frac{E}{L}bS_i & \frac{E}{L}bS_{i+1} \\ 0 & 0 & 1 & 0 & 0 & 0 & 0 & 0 & 0 \\ e_{3i} & e_{2i} & e_{4i} & 0 & 0 & 0 & e_{1i} & 0 & 0 \\ 0 & 0 & 0 & -\frac{1}{\tau_{\text{d},i,i+1}} & 0 & 0 & 0 & 0 & 0 \\ 0 & 0 & 0 & 0 & -\frac{1}{\tau_{V,i}} & 0 & 0 & 0 & 0 \\ 0 & 0 & 0 & 0 & 0 & -\frac{1}{\tau_{V,i+1}} & 0 & 0 & 0 \\ 0 & 0 & 0 & 0 & 0 & 0 & -\frac{1}{\tau_{M,i}} & 0 & 0 \\ 0 & 0 & 0 & 0 & 0 & 0 & 0 & -\frac{1}{\tau_{S,i}} & 0 \\ 0 & 0 & 0 & 0 & 0 & 0 & 0 & 0 & -\frac{1}{\tau_{S,i+1}} \end{bmatrix}$$

$$\boldsymbol{B}_i = \begin{bmatrix} 0 & 0 & 0 & 0 & 0 \\ 0 & 0 & 0 & 0 & 0 \\ 0 & 0 & 0 & 0 & 0 \\ 0 & 0 & 0 & 0 & 0 \\ \frac{1}{\tau_{V,i}} & 0 & 0 & 0 & 0 \\ 0 & \frac{1}{\tau_{V,i+1}} & 0 & 0 & 0 \\ 0 & 0 & \frac{1}{\tau_{M,i}} & 0 & 0 \\ 0 & 0 & 0 & \frac{1}{\tau_{S,i}} & 0 \\ 0 & 0 & 0 & 0 & \frac{1}{\tau_{S,i+1}} \end{bmatrix}$$

$$\boldsymbol{C}_i = \begin{bmatrix} 0 & 1 & 0 & 0 & 0 & 0 & 0 & 0 & 0 \\ 1 & 0 & 0 & 0 & 0 & 0 & 0 & 0 & 0 \\ a\sigma_{\text{out},i} & 0 & 0 & 0 & a_{\omega,i} & 0 & 0 & a_{S,i} & 0 \end{bmatrix}$$

$$\boldsymbol{D}_{\text{in},i} = \begin{bmatrix} bh_{\text{in},i} & bh_{\text{in},i+1} & b\sigma_{\text{in},i} & b\sigma_{\text{out},i+1} & bT_i \\ 0 & 0 & 0 & 0 & 0 \\ 0 & 0 & 0 & 0 & 0 \\ 0 & 0 & 0 & 0 & 0 \\ 0 & 0 & 0 & 0 & 0 \\ 0 & 0 & 0 & 0 & 0 \\ 0 & 0 & 0 & 0 & 0 \\ 0 & 0 & 0 & 0 & 0 \\ 0 & 0 & 0 & 0 & 0 \end{bmatrix}$$

$$\boldsymbol{D}_{\text{out},i} = \begin{bmatrix} 0 & 0 & 0 & 0 & 0 \\ 0 & 0 & 0 & 0 & 0 \\ ah_{\text{in},i} & 0 & a\sigma_{\text{in},i} & 0 & aT_i \end{bmatrix}$$

signal $\Delta \boldsymbol{U}_i$ in the predictive horizon N_c can be expressed as follows:

$$\Delta \boldsymbol{U}_i = \begin{bmatrix} \Delta \boldsymbol{u}_i(k_n) \\ \Delta \boldsymbol{u}_i(k_n+1) \\ \vdots \\ \Delta \boldsymbol{u}_i(k_n+N_c-1) \end{bmatrix} \tag{58}$$

In an actual AGC-LP integrated system, the saturation in the controller input and the increment limits in the actuator should be considered. Hence, the incremental constraints for the control variables are designed as follows:

$$\Delta \boldsymbol{u}_i^{\min} \le \Delta \boldsymbol{u}_i(k) \le \Delta \boldsymbol{u}_i^{\max} \tag{59}$$

In the predictive horizon N_c, Eq. (59) can be expressed as follows:

$$\begin{bmatrix} \Delta \boldsymbol{u}_i^{\min} \\ \Delta \boldsymbol{u}_i^{\min} \\ \vdots \\ \Delta \boldsymbol{u}_i^{\min} \end{bmatrix} \le \begin{bmatrix} \Delta \boldsymbol{u}_i\,(k_n) \\ \Delta \boldsymbol{u}_i\,(k_n+1) \\ \vdots \\ \Delta \boldsymbol{u}_i\,(k_n+N_c-1) \end{bmatrix} \le \begin{bmatrix} \Delta \boldsymbol{u}_i^{\max} \\ \Delta \boldsymbol{u}_i^{\max} \\ \vdots \\ \Delta \boldsymbol{u}_i^{\max} \end{bmatrix} \tag{60}$$

$$\Delta \boldsymbol{U}_i^{\min} \le \Delta \boldsymbol{U}_i \le \Delta \boldsymbol{U}_i^{\max} \tag{61}$$

The state variable and output variable of the AGC-LP integrated system can be written as follows:

$$\boldsymbol{X}_i = \begin{bmatrix} \boldsymbol{x}_i(k_n+1|k_n) \\ \boldsymbol{x}_i(k_n+2|k_n) \\ \vdots \\ \boldsymbol{x}_i(k_n+m|k_n) \\ \vdots \\ \boldsymbol{x}_i(k_n+N_p|k_n) \end{bmatrix}, \quad \boldsymbol{Y}_i = \begin{bmatrix} \boldsymbol{y}_i(k_n+1|k_n) \\ \boldsymbol{y}_i(k_n+2|k_n) \\ \vdots \\ \boldsymbol{y}_i(k_n+m|k_n) \\ \vdots \\ \boldsymbol{y}_i(k_n+N_p|k_n) \end{bmatrix} \tag{62}$$

where $\boldsymbol{x}_i(k_n+m|k_n)$are the predicted state variables at time k_n+m and $\boldsymbol{y}_i(k_n+m|k_n)$ are the predicted output variables at time k_n+m.

There is an iterative relationship between the predicted state variables and output variables, which can be expressed as follows:

$$\begin{aligned}
\boldsymbol{x}_i(k_n+1|k_n) &= \boldsymbol{A}_i\boldsymbol{x}_i(k_n) + \boldsymbol{D}_i\boldsymbol{d}_i(k_n) + \boldsymbol{B}_i\Delta\boldsymbol{u}_i(k_n) \\
\boldsymbol{x}_i(k_n+2|k_n) &= \boldsymbol{A}_i^2\boldsymbol{x}_i(k_n) + \boldsymbol{D}_i^2\boldsymbol{d}_i(k_n) + \boldsymbol{A}_i\boldsymbol{B}_i\Delta\boldsymbol{u}_i(k_n) \\
&\quad + \boldsymbol{B}_i\Delta\boldsymbol{u}_i(k_n+1) \\
&\vdots \\
\boldsymbol{x}_i(k_n+N_c|k_n) &= \boldsymbol{A}_i^{N_c}\boldsymbol{x}_i(k_n) + \boldsymbol{D}_i^{N_c}\boldsymbol{d}_i(k_n) + \boldsymbol{A}_i^{N_c-1}\boldsymbol{B}_i\Delta\boldsymbol{u}_i(k_n) \\
&\quad + \cdots \boldsymbol{A}_i\boldsymbol{B}_i\Delta\boldsymbol{u}_i(k_n+N_c-2) \\
&\quad + \boldsymbol{B}_i\Delta\boldsymbol{u}_i(k_n+N_c-1) \\
&\vdots \\
\boldsymbol{x}_i(k_n+N_p|k_n) &= \boldsymbol{A}_i^{N_p}\boldsymbol{x}_i(k_n) + \boldsymbol{D}_i^{N_p}\boldsymbol{d}_i(k_n) + \boldsymbol{A}_i^{N_p-1}\boldsymbol{B}_i\Delta\boldsymbol{u}_i(k_n) \\
&\quad + \cdots \boldsymbol{A}_i^{N_p-N_c+1}\boldsymbol{B}_i\Delta\boldsymbol{u}_i(k_n+N_c-2) \\
&\quad + \boldsymbol{A}_i^{N_p-N_c}\boldsymbol{B}_i\Delta\boldsymbol{u}_i(k_n+N_c-1)
\end{aligned}$$

Then, the output sequences of the AGC-LP integrated system can be obtained as follows:

$$\boldsymbol{Y}_i = \boldsymbol{F}_i\boldsymbol{x}_i\,(k_n) + \boldsymbol{G}_i\boldsymbol{d}_i(k_n) + \boldsymbol{\psi}_i\Delta\boldsymbol{U} \tag{63}$$

where

$$\boldsymbol{F}_i = \begin{bmatrix} \boldsymbol{C}_i\boldsymbol{A}_i \\ \boldsymbol{C}_i\boldsymbol{A}_i^2 \\ \vdots \\ \boldsymbol{C}_i\boldsymbol{A}_i^{N_c} \\ \vdots \\ \boldsymbol{C}_i\boldsymbol{A}_i^{N_p} \end{bmatrix}, \quad \boldsymbol{G}_i = \begin{bmatrix} \boldsymbol{D}_i\boldsymbol{A}_i \\ \boldsymbol{D}_i\boldsymbol{A}_i^2 \\ \vdots \\ \boldsymbol{D}_i\boldsymbol{A}_i^{N_c-2} \\ \vdots \\ \boldsymbol{D}_i\boldsymbol{A}_i^{N_p-2} \end{bmatrix},$$

$$\boldsymbol{\psi}_i = \begin{bmatrix} \boldsymbol{C}_i\boldsymbol{B}_i & \boldsymbol{0} & \boldsymbol{0} & \boldsymbol{0} \\ \boldsymbol{C}_i\boldsymbol{A}_i\boldsymbol{B}_i & \boldsymbol{C}_i\boldsymbol{B}_i & \boldsymbol{0} & \boldsymbol{0} \\ \vdots & \ddots & \ddots & \boldsymbol{0} \\ \boldsymbol{C}_i\boldsymbol{A}_i^{N_c-1}\boldsymbol{B}_i & \cdots & \boldsymbol{C}_i\boldsymbol{A}_i\boldsymbol{B}_i & \boldsymbol{C}_i\boldsymbol{B}_i \\ \vdots & \vdots & \vdots & \vdots \\ \boldsymbol{C}_i\boldsymbol{A}_i^{N_p-1}\boldsymbol{B}_i & \cdots & \boldsymbol{C}_i\boldsymbol{A}_i^{N_p-N_c+1}\boldsymbol{B}_i & \boldsymbol{C}_i\boldsymbol{A}_i^{N_p-N_c}\boldsymbol{B}_i \end{bmatrix}$$

The related constraints are also required for the output of the AGC-LP integrated system, which is designed as follows:

$$\boldsymbol{Y}_i^{\min} \le \boldsymbol{Y}_i \le \boldsymbol{Y}_i^{\max} \tag{64}$$

According to Eq. (63), Eq. (64) can be rewritten as follows:

$$\begin{aligned}
&\boldsymbol{Y}^{\min} - \boldsymbol{F}_i\boldsymbol{x}_i\,(k_n) - \boldsymbol{G}_i\boldsymbol{d}_i(k_n) \\
&\qquad \le \boldsymbol{\psi}_i\Delta\boldsymbol{U}_i \le \boldsymbol{Y}^{\max} - \boldsymbol{F}_i\boldsymbol{x}_i\,(k_n) - \boldsymbol{G}_i\boldsymbol{d}_i(k_n)
\end{aligned} \tag{65}$$

The performance index function for the DMPC controller is defined as follows:

$$\boldsymbol{J}_i = \left(\boldsymbol{R}_i^s - \boldsymbol{Y}_i\right)^{\mathrm{T}} \bar{\boldsymbol{Q}}_i \left(\boldsymbol{R}_i^s - \boldsymbol{Y}_i\right) + \Delta\boldsymbol{U}^{\mathrm{T}}\bar{\boldsymbol{R}}_i\Delta\boldsymbol{U} \tag{66}$$

where $\boldsymbol{R}_i^s$ is the set value of the output trajectory and $\bar{\boldsymbol{Q}}_i$ and $\bar{\boldsymbol{R}}_i$ are the weight matrices.

By substituting Eq. (63) into Eq. (66), the performance index function can be rewritten as follows:

$$\begin{aligned}
\boldsymbol{J}_i = &\left[\boldsymbol{R}_i^s - \boldsymbol{F}_i\boldsymbol{x}_i(k_n) - \boldsymbol{G}_i\boldsymbol{d}_i(k_n)\right]^{\mathrm{T}} \\
&\times \bar{\boldsymbol{Q}}_i\left[\boldsymbol{R}_i^s - \boldsymbol{F}_i\boldsymbol{x}_i(k_n) - \boldsymbol{G}_i\boldsymbol{d}_i(k_n)\right] \\
&- 2\Delta\boldsymbol{U}_i^{\mathrm{T}}\boldsymbol{\psi}_i^{\mathrm{T}}\bar{\boldsymbol{Q}}_i\left[\boldsymbol{R}_i^s - \boldsymbol{F}_i\boldsymbol{x}_i(k_n) - \boldsymbol{G}_i\boldsymbol{d}_i(k_n)\right] \\
&+ \Delta\boldsymbol{U}_i^{\mathrm{T}}\left(\boldsymbol{\psi}_i^{\mathrm{T}}\bar{\boldsymbol{Q}}_i\boldsymbol{\psi}_i + \bar{\boldsymbol{R}}_i\right)\Delta\boldsymbol{U}_i
\end{aligned} \tag{67}$$

The optimal control sequences can be obtained by the sequential quadratic programming method as follows:

$$\min\ \boldsymbol{J}_i = \frac{1}{2}\boldsymbol{\eta}_i^T\boldsymbol{E}_i\boldsymbol{\eta}_i + \boldsymbol{\eta}_i^T\boldsymbol{G}_i \tag{68}$$

$$s.t.\ \Delta\boldsymbol{U}_i^{\min} \le \Delta\boldsymbol{U}_i \le \Delta\boldsymbol{U}_i^{\max} \tag{69}$$

$$s.t.\ \boldsymbol{Y}_i^{\min} \le \boldsymbol{Y}_i \le \boldsymbol{Y}_i^{\max} \tag{70}$$

where

$$\begin{aligned}
\boldsymbol{\eta}_i &= \Delta\boldsymbol{U}_i, \quad \boldsymbol{E} = \boldsymbol{\psi}_i^{\mathrm{T}}\bar{\boldsymbol{Q}}_i\boldsymbol{\psi}_i + \bar{\boldsymbol{R}}_i, \\
\boldsymbol{G}_i &= -2\boldsymbol{\psi}_i^{\mathrm{T}}\bar{\boldsymbol{Q}}_i\left[\boldsymbol{R}_i^s - \boldsymbol{F}_i\boldsymbol{x}_i\,(k_n)\right]
\end{aligned}$$

Then, the optimal control sequences can be calculated as follows:

$$\Delta\boldsymbol{U}_i^* = \left(\boldsymbol{\psi}_i^{\mathrm{T}}\bar{\boldsymbol{Q}}_i\boldsymbol{\psi}_i + \bar{\boldsymbol{R}}_i\right)^{-1}\boldsymbol{\psi}_i^{\mathrm{T}}\bar{\boldsymbol{Q}}_i\left[\boldsymbol{R}_i^s - \boldsymbol{F}_i\boldsymbol{x}_i(k_n) - \boldsymbol{G}_i\boldsymbol{d}_i(k_n)\right] \tag{71}$$

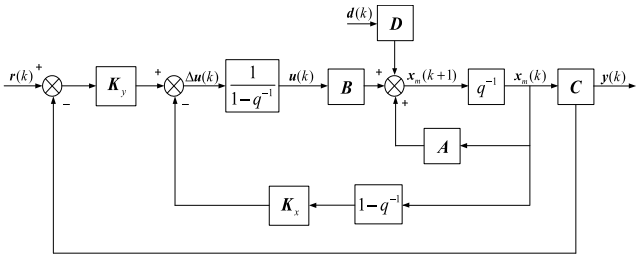

FIGURE 6. Structure diagram of the DMPC scheme based on the augmented minimal state-space.

According to the principle of moving horizon estimation, the first element of $\Delta \boldsymbol{U}_i$can be treated as the control increment for time k_n:

$$\begin{aligned}\Delta \boldsymbol{u}(k_n) &= \overbrace{\begin{bmatrix}1 & 0 & 0 & \cdots & 1\end{bmatrix}}^{N_c}\left(\boldsymbol{\psi}_i^{\mathrm{T}}\bar{\boldsymbol{Q}}_i\boldsymbol{\psi}_i+\bar{\boldsymbol{R}}_i\right)^{-1}\\ &\quad\times\boldsymbol{\psi}_i^{\mathrm{T}}\bar{\boldsymbol{Q}}_i\left[\bar{\boldsymbol{R}}_i^s\boldsymbol{r}_i(k_n)-\boldsymbol{F}_i\boldsymbol{x}_i(k_n)-\boldsymbol{G}_i\boldsymbol{d}_i(k_n)\right]\\ &= \boldsymbol{K}_y\boldsymbol{r}_i(k_n)-\boldsymbol{K}_d\boldsymbol{d}_i(k_n)-\boldsymbol{K}_{mpc}\boldsymbol{x}_i(k_n)\end{aligned} \tag{72}$$

where $\boldsymbol{K}_y$ is the first element in $\left(\boldsymbol{\psi}_i^{\mathrm{T}}\bar{\boldsymbol{Q}}_i\boldsymbol{\psi}_i+\bar{\boldsymbol{R}}_i\right)^{-1}\boldsymbol{\psi}_i^{\mathrm{T}}\bar{\boldsymbol{Q}}_i\bar{\boldsymbol{R}}_i^s$, $\boldsymbol{K}_d$ is the first element in $\left(\boldsymbol{\psi}_i^{\mathrm{T}}\bar{\boldsymbol{Q}}_i\boldsymbol{\psi}_i+\bar{\boldsymbol{R}}_i\right)^{-1}\boldsymbol{\psi}_i^{\mathrm{T}}\bar{\boldsymbol{Q}}_i\boldsymbol{G}_i$, and $\boldsymbol{K}_{mpc}$ is the first element in $\left(\boldsymbol{\psi}_i^{\mathrm{T}}\bar{\boldsymbol{Q}}_i\boldsymbol{\psi}_i+\bar{\boldsymbol{R}}_i\right)^{-1}\boldsymbol{\psi}_i^{\mathrm{T}}\bar{\boldsymbol{Q}}_i\boldsymbol{F}_i$.

According to Eq. (57) and Eq. (72), the state equation of the DMPC controller can be obtained as follows:

$$\boldsymbol{x}_i(k+1)=\left(\boldsymbol{A}_i-\boldsymbol{B}_i\boldsymbol{K}_{mpc}\right)\boldsymbol{x}_i(k)+\boldsymbol{B}_i\boldsymbol{K}_y\boldsymbol{r}_i(k)+\boldsymbol{D}_i\boldsymbol{K}_d\boldsymbol{d}_i(k) \tag{73}$$

As a special structure of matrices $\boldsymbol{A}_i$ and $\boldsymbol{C}_i$, the last column of $\boldsymbol{F}_i$ is equal to $\boldsymbol{R}_i^s$, and the last element of $\boldsymbol{K}_y$ is same as the last element of $\boldsymbol{K}_{mpc}$. The state variables $\boldsymbol{x}(k) = \begin{bmatrix}\Delta \boldsymbol{x}_m(k) & \boldsymbol{y}(k)\end{bmatrix}^T$, and the gain vector of state feedback matrix $\boldsymbol{K}_{mpc}$ can be expressed as follows:

$$\boldsymbol{K}_{mpc} = \begin{bmatrix}\boldsymbol{K}_x & \boldsymbol{K}_y\end{bmatrix} \tag{74}$$

where $\boldsymbol{K}_y$ is the state feedback gain vector for $y(k)$ and $\boldsymbol{K}_x$ is the state feedback gain vector for $\Delta \boldsymbol{x}_m(k)^T$. The DMPC scheme based on the augmented minimal state-space can be described as shown in Figure 6:

B. DESIGN OF THE DMPC CONTROLLER FOR THE AGC-LP INTERGRATED SYSTEM

According to the DMPC design theory presented above, Eq. (52) is discretized at the sample time $q = 0.005$ s. The related parameters are selected according to the literature [24], and the discrete state-space model of the AGC-LP integrated system can be obtained as follows:

$$\begin{cases}\bar{\boldsymbol{x}}_i(k+1)=\bar{\boldsymbol{A}}_i\bar{\boldsymbol{x}}_i(k)+\bar{\boldsymbol{B}}_i\bar{\boldsymbol{u}}_i(k)+\bar{\boldsymbol{D}}_i\bar{\boldsymbol{d}}_i(k)\\ \bar{\boldsymbol{y}}_i(k)=\bar{\boldsymbol{C}}_i\bar{\boldsymbol{x}}_i(k)\end{cases} \tag{75}$$

where, $\bar{\boldsymbol{A}}_i$, as shown at the bottom of the next page,

The improved minimal state-space of the AGC-LP integrated system corresponding with Eq. (56) can be established as follows:

$$\begin{cases}\boldsymbol{x}_i(k+1)=\boldsymbol{A}_i\boldsymbol{x}_i(k)+\boldsymbol{B}_i\boldsymbol{u}_i(k)+\boldsymbol{D}_i\boldsymbol{d}_i(k)\\ \boldsymbol{y}_i(k)=\boldsymbol{C}_i\boldsymbol{x}_i(k)\end{cases} \tag{76}$$

Based on the dynamic characteristics of the AGC-LP integrated system, the number of prediction steps N_p and control steps N_c are set to 5 and 3, respectively, and the weighting matrices are designed as follows:

$$\bar{\boldsymbol{Q}}_i=\begin{bmatrix}\bar{\boldsymbol{Q}}_{1i} & 0 & 0\\ 0 & \ddots & 0\\ 0 & 0 & \bar{\boldsymbol{Q}}_{1i}\end{bmatrix}_{3N_p\times 3N_p}\qquad \bar{\boldsymbol{R}}_i=\begin{bmatrix}\bar{\boldsymbol{R}}_{1i} & 0 & 0\\ 0 & \ddots & 0\\ 0 & 0 & \bar{\boldsymbol{R}}_{1i}\end{bmatrix}_{3N_c\times 3N_c}$$

where

$$\bar{\boldsymbol{Q}}_{1i}=\begin{bmatrix}300 & 0 & 0\\ 0 & 300 & 0\\ 0 & 0 & 3\end{bmatrix}\qquad \bar{\boldsymbol{R}}_{1i}=\begin{bmatrix}0.1 & 0 & 0\\ 0 & 0.1 & 0\\ 0 & 0 & 0.1\end{bmatrix}$$

The related constraints added to the increments of the control input and system output are designed as follows:

$$\begin{aligned}|\Delta u_{\Delta\omega}| &\le 0.1 \text{ rad/s} \quad |\Delta u_{\Delta M}| \le 5000 \text{ kNm}\\ |\Delta u_{\Delta S}| &\le 0.05 \text{ mm} \quad |\Delta\theta| \le 0.02 \text{ rad}\\ |\Delta\sigma| &\le 1 \text{ MPa} \quad |\Delta h_{i+1}| \le 0.03 \text{ mm}\end{aligned}$$

According to information presented above, all the gain vectors of the state feedback control can be calculated as follows:

$$\begin{aligned}\boldsymbol{K}_x &= [38.8572 \quad 23.2354 \quad 1.2358 \quad -0.0505 \quad 0.0772\\ &\quad\ 2.8325 \quad 14.5236 \quad 7.8421]\\ \boldsymbol{K}_y &= [10.5236]\\ \boldsymbol{K}_{mpc} &= [38.8572 \quad 23.2354 \quad 1.2358 \quad -0.0505\\ &\quad\ 0.0772 \quad 2.8325 \quad 14.5236 \quad 7.8421 \quad 10.5236]\end{aligned}$$

IV. SIMULATION EXPERIMENTS AND DISUSSION

To verify the good performance of the designed DMPC controller, the control systems for the 6th-stand and 7th-stand were established based on the PI control scheme and DMPC control scheme. Then, simulation analyses for the response performance, disturbance rejection performance and robustness of both control schemes were performed by MATLAB/Simulink.

A. RESPONSE PERFORMANCE COMPARISON

During the hot strip rolling process, the control accuracy of the LP system and AGC system directly affects the tension stability and dimensional precision of the strip. To study the control accuracy of the PI controller and DMPC controller, a step testing signal was added to the initial value of the strip gauge, looper angle and strip tension, and the dynamic characteristic parameters of the DMPC controller and PI controller were compared.

1) A step testing signal with an amplitude of 0.03 mm was added to the initial value of the strip gauge at $t = 3$ s, and the simulation results are shown in Figure 7.

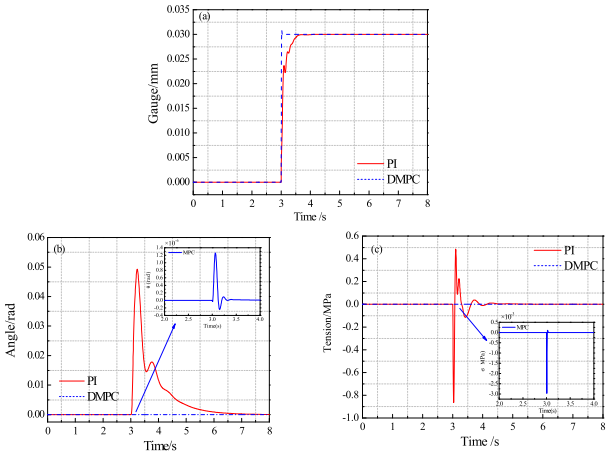

FIGURE 7. System outputs in response to a step disturbance in the strip gauge: (a) gauge, (b) angle, and (c) tension.

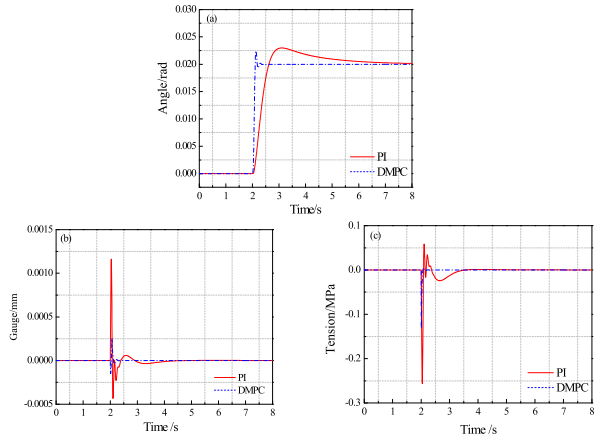

FIGURE 8. System outputs in response to a step disturbance in the looper angle: (a) angle, (b) gauge, and (c) tension.

2) A step testing signal with an amplitude of 0.02 rad was added to the initial value of the looper angle at t=2 s, and the simulation results are shown in Figure 8.

3) A step testing signal with an amplitude of 1.0 MPa was added to the initial value of the strip tension at $t = 1$ s, and the simulation results are shown in Figure 9.

The dynamic characteristic parameters of the PI controller and DMPC controller were again calculated, and the results are shown in Table 1.

As shown in the Table 1, for the PI controller, the rising time of the gauge reaches 472.5 ms, the rising time of the angle reaches 732.5 ms, and the overshoot of the tension reaches 18.23%. These dynamic characteristic parameters are unacceptable for a hot strip mill control system. However, for the DMPC controller, the rising time of the strip gauge, looper angle and strip tension are only 16.5 ms, 64.5 ms and 24.5 ms, respectively, which are acceptable for a hot strip mill control system. Furthermore, the gauge, angle and tension are coordinate-controlled in the DMPC controller. When inputting a step signal, the fluctuations in the other parameters are much smaller than those in the PI controller.

B. DISTURBANCE REJECTION PERFORMANCE COMPARISON

The incoming strip thickness fluctuation, incoming strip temperature fluctuation, and roll eccentricity are the most

$$\bar{\boldsymbol{A}}_i = \begin{bmatrix} 0.9735 & 0.0149 & -0.0336 & 0.4547 & 5.16e-5 & -5.703e-4 \\ -0.6071 & -0.1216 & 0.0844 & 12.753 & 2.2736e-4 & -0.011 \\ -0.22 & -0.0135 & -0.0764 & 0.6355 & 2.3474e-4 & -0.0021 \\ 0 & 0 & 0 & 0.6593 & 0 & 0 \\ 0 & 0 & 0 & 0 & 0.0821 & 0 \\ 0 & 0 & 0 & 0 & 0 & 0.1889 \end{bmatrix}$$

$$\bar{\boldsymbol{B}}_i = \begin{bmatrix} 0.0678 & 7.0767e-5 & -3.7806e-4 \\ 3.7893 & 0.0026 & -0.019 \\ -0.5361 & 7.8282e-4 & 0.0019 \\ 0.3407 & 0 & 0 \\ 0 & 0.9179 & 0 \\ 0 & 0 & 0.8111 \end{bmatrix}$$

$$\bar{\boldsymbol{C}}_i = \begin{bmatrix} 1 & 0 & 0 & 0 & 0 & 0 \\ 0 & 0 & 1 & 0 & 0 & 0 \\ 0 & 0 & -16.29 & 0 & 0 & 0.334 \end{bmatrix}$$

$$\bar{\boldsymbol{D}}_i = \begin{bmatrix} 0 & 0 \\ 0 & 0 \\ -0.1872 & -15.81 \\ 0 & 0 \\ 0 & 0 \\ 0 & 0 \end{bmatrix}$$

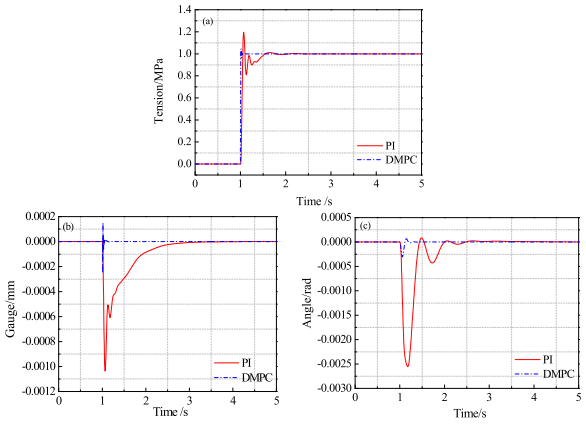

FIGURE 9. System outputs in response to a step disturbance in the strip tension: (a) tension, (b) gauge, and (c) angle.

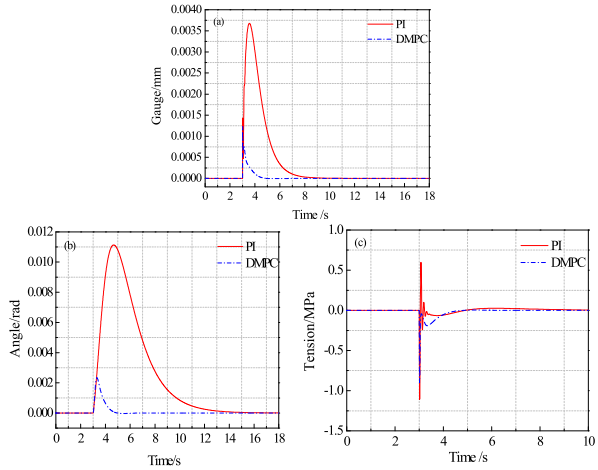

FIGURE 10. System outputs in response to a step disturbance in the incoming strip thickness: (a) gauge, (b) angle, and (c) tension.

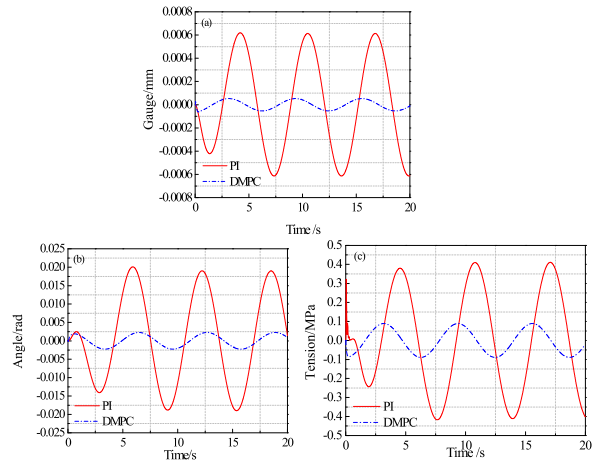

FIGURE 11. System outputs in response to a sinusoidal disturbance in the incoming strip temperature: (a) gauge, (b) angle, and (c) tension.

common disturbances during the hot strip rolling process. To study the disturbance rejection performance of the PI controller and DMPC controller, disturbance signals were added

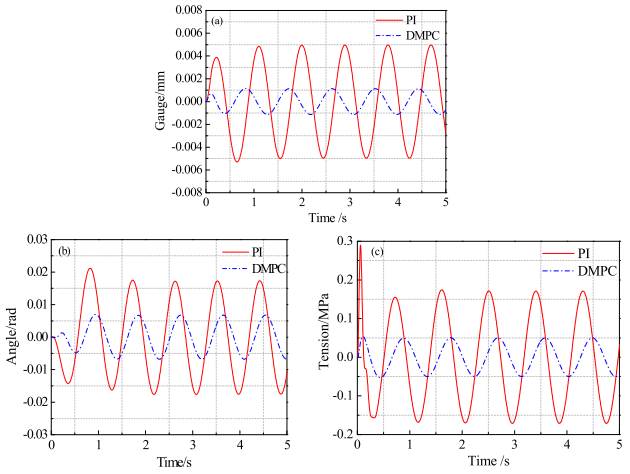

FIGURE 12. System outputs in response to a sinusoidal disturbance in the roll eccentricity: (a) gauge, (b) angle, and (c) tension.

TABLE 1. Dynamic characteristic parameters of the PI controller and DMPC controller.

Paramete r / Controller		Rising time	Overshoot	Fluctuation
Step-gauge	PI	472.5 ms	1.32%	0.048 rad/1.36 MPa
	DMPC	16.5 ms	2.76%	1.3e-6 rad/3.1e-3 MPa
Step-angle	PI	732.5 ms	13.52%	1.76 μm/0.277 MPa
	DMPC	64.5 ms	12.23%	0.34 μm/0.135 MPa
Step-tension	PI	123.5 ms	18.23%	1.03 μm/2.72e-3 rad
	DMPC	24.5 ms	2.242%	0.33 μm/2.62e-4 rad

to the incoming strip thickness, incoming strip temperature and roll gap. Finally, the disturbance rejection performance of the PI controller and DMPC controller were compared based on the dynamic characteristic parameters obtained by the simulation.

1) A step testing signal with an amplitude of 0.05 mm was added to the initial value of the incoming strip gauge at $t = 3$ s, and the simulation results are shown in Figure 10.

2) A sinusoidal testing signal with an amplitude of 10° and a frequency of 0.2 Hz was added to the initial value of the incoming strip temperature at t=2 s, and the simulation results are shown in Figure 11.

3) A sinusoidal testing signal with an amplitude of 0.025 mm and a frequency of 1.0 Hz was added to the initial value of the 7th roll gap, and the simulation results are shown in Figure 12.

The dynamic characteristic parameters of the PI controller and DMPC controller were again calculated, and the results are presented in Table 2.

As shown in Table 2, when the hot strip mill encounters fluctuations in the incoming strip thickness, incoming strip temperature and roll eccentricity, there is substantial coupling among the strip gauge, looper angle and strip tension. The gauge fluctuations given by the PI controller are 3.73e-3 mm,

TABLE 2. Dynamic characteristic parameters of the PI controller and DMPC controller.

Parameter / Controller		Gauge fluctuation	Angle fluctuation	Tension fluctuation
Strip gauge fluctuation	PI	3.73e-3 mm	1.13e-2 rad	1.353 MPa
	DMPC	1.24e-3 mm	2.87e-3 rad	8.57e-1 MPa
Strip temperature fluctuation	PI	1.26e-3 mm	4.06e-2 rad	8.23e-1 MPa
	DMPC	1.16e-4 mm	4.47e-3 rad	1.71e-1 MPa
Roller eccentricity	PI	1.04e-2 mm	3.98e-2 rad	4.71e-1 MPa
	DMPC	2.94e-3 mm	2.01e-2 rad	1.14e-1 MPa

TABLE 3. Dynamic characteristic parameters of the PI controller and DMPC controller.

Controller	S=1448 mm^2		S=2230 mm^2		S=4952mm^2		S=7825mm^2	
	PI	DMPC	PI	DMPC	PI	DMPC	PI	DMPC
Rising time/ms	478.3	17.2	473.2	17.4	469.4	17.0	467.1	16.4
Gauge overshoot/%	1.24	2.64	1.26	2.58	1.34	2.37	1.32	2.66
Tension fluctuation/MPa	1.98	3.1e-3	1.72	3.1e-3	1.28	3.0e-3	1.17	2.9e-3
Angle fluctuation/rad	0.044	1.2e-6	0.034	1.3e-6	0.021	1.3e-6	0.013	1.4e-6

1.26e-3 mm and 1.04e-2 mm. The angle fluctuations given by the PI controller are 1.31e-2 rad, 4.06e-2 rad and 3.98e-2 rad. The tension fluctuations given by the PI controller are 1.353 MPa, 8.23e-1 MPa and 4.71e-1 MPa. As the on-line rolling optimization strategy and feedback correction strategy was designed in the DMPC controller, the disturbances can be corrected rapidly, and the fluctuation in all parameters can be controlled in a small region. Hence, the DMPC controller can increase the disturbance rejection performance of the AGC-LP integrated system.

C. ROBUSTNESS COMPARISON

Steel strips with many different specifications are produced in an actual hot strip mill, and the model mismatch caused by the change in strip specifications substantially affects the dynamic characteristic parameters of the system. To study the robustness of the PI controller and DMPC controller, the dynamic response characteristic of both controllers were simulated under the condition that the cross-sectional area of the strip $\boldsymbol{S}$ changes.

1) Under the condition that the cross-sectional area of the strip $\boldsymbol{S}$ changes, a step testing signal with an amplitude of 0.03 mm was added to the initial value of the strip gauge at t=2 s, and the simulation results are shown in Figure 13.

The dynamic characteristic parameters of the PI controller and DMPC controller were again calculated, and the results are presented in Table 3.

2) A step testing signal with an amplitude of 1.0 MPa was added to the initial value of the strip tension at t=1 s, and the simulation results are shown in Figure 14.

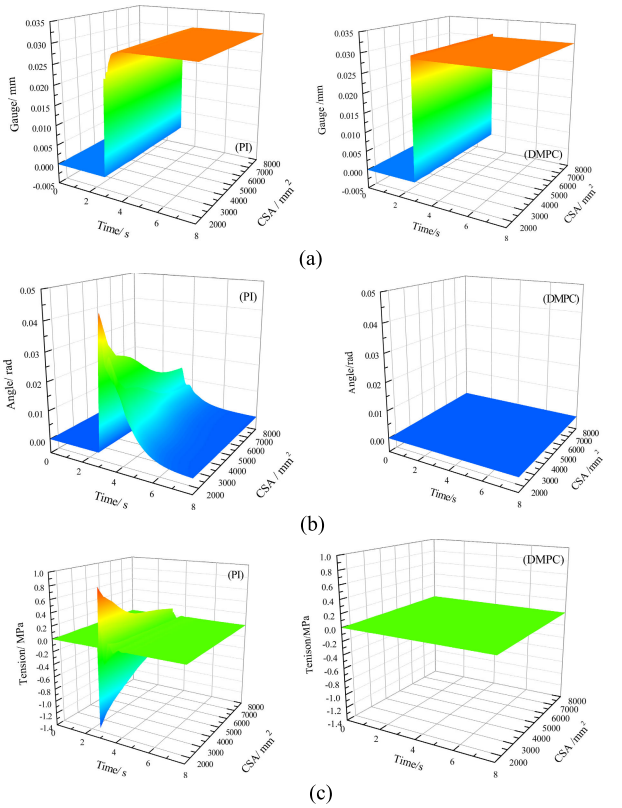

FIGURE 13. (a) Output curves of gauge with varying cross-sectional area in response to a step gauge change. (b) Output curves of angle with varying cross-sectional area in response to a step gauge change. (c) Output curves of tension with varying cross-sectional area in response to a step gauge change.

TABLE 4. Dynamic characteristic parameters of the PI controller and DMPC controller.

Controller	S=1448 mm^2		S=2230 mm^2		S=4952mm^2		S=7825mm^2	
	PI	DMPC	PI	DMPC	PI	DMPC	PI	DMPC
Rising time/ms	128.8	24.8	130.4	24.3	147.6	25.6	212.5	24.5
Gauge overshoot/%	41.21	2.232	35.4	2.183	0.823	2.137	0.237	2.242
Tension fluctuation/MPa	4.32	0.28	3.25	0.28	2.28	0.27	1.73	0.28
Angle fluctuation/rad	1.17	0.38	1.12	0.35	0.98	0.35	0.95	0.37

The dynamic characteristic parameters of the PI controller and DMPC controller were again calculated, and the results are presented in Table 4.

As shown in the simulation results presented above, when the cross-sectional area of the strip $\boldsymbol{S}$ changes, the robustness of the PI controller decreases, and large overshoots or long rising times appear. However, the AGC-LP integrated system based on the proposed DMPC controller is relatively insensitive to the rolling condition changes and model mismatch. When a step testing signal was added to the initial value of the strip tension, the PI controller had an overshoot in tension of 41.21%, wherein the proposed DMPC controller had an overshoot of only 2.232%. Moreover, when a step testing signal was added to the initial value of the strip

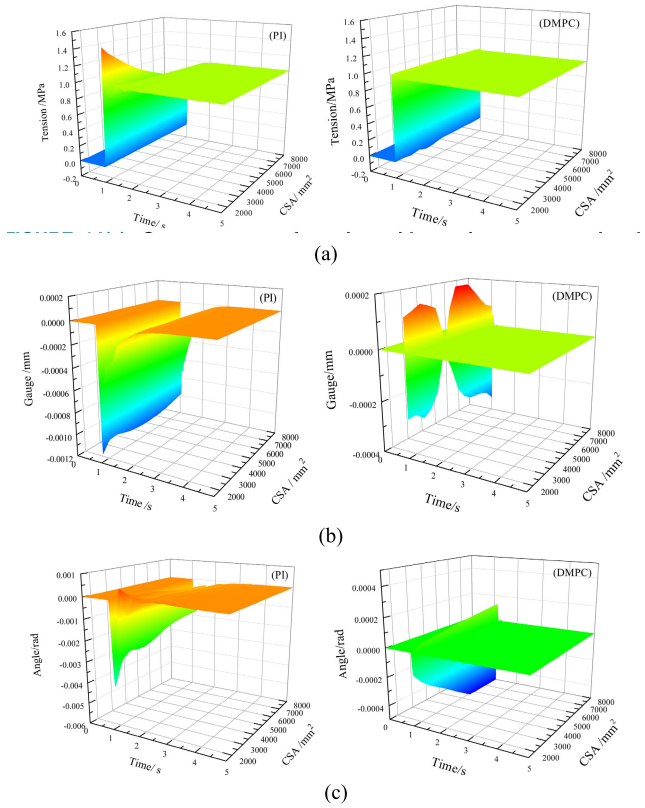

FIGURE 14. (a) Output curves of tension with varying cross-sectional area in response to a step tension change. (b) Output curves of gauge with varying cross-sectional area in response to a step tension change. (c) Output curves of angle with varying cross-sectional area in response to a step tension change.

gauge, the rising time of the PI controller fluctuated in the range of 478.3 ms to 467.1 ms, whereas the rising time of the DMPC controller was less than 18 ms in all cases. The results presented above clearly show that, compared to the PI controller, the DMPC controller is more robust and can provide a better control effect for the strip gauge, looper angle and strip tension.

V. CONCLUSION

In this paper, according to hot rolling theory, a state-space model of a hot strip mill was established that considers the coupling relationship between the AGC and LP systems, the thickness delay, and the temperature delay. As expected, there was only a small difference between the real data and the results from the established model. In addition, based on the established AGC-LP state-space model, a DMPC controller was designed for coordinative optimization of the strip gauge, looper angle and strip tension in a hot strip mill. Finally, the simulation analyses were performed to compare the response performance, disturbance rejection performance and robustness performance of the traditional PI controller and the proposed DMPC controller. The simulation results showed that the overshoot and rising time of the PI controller failed to meet acceptable levels for a hot strip mill system in cases of model mismatch. Future work will include modeling of parametric uncertainties and application of nonlinear control schemes for hot strip mills.

NOTATION

ρ_C	-carbon content in the strip/%;
ε	-relative deformation degree/%;
ω	- roll rotation speed/(rad/s);
R'	- deformed working roller radius/mm;
H	-entry thickness of the strip/mm;
h	-exit thickness of the strip/mm;
T	-rolled workpiece temperature/°C;
t_d^o	-phase transition temperature/°C;
σ_s	-Stefan-Boltzmann constant;
W	- strip width/mm;
l	-strip length/mm;
ρ	- strip density/(kg/m^3);
C	-specific heat capacity of the strip/J/(kg·°);
k_{T}	-cooling efficiency;
T_{w}	-cooling water temperature/°;
f_{s}	- nozzle flow/(m^3/s);
p	-nozzle pressure/MPa;
v	-strip speed/(m/s);
p_c	- average unit pressure/MPa;
η	- absorption efficiency/%;
l_c	-length of the contact arc/mm;
β	- thermal conductivity efficiency/%;
T_{roll}	-temperature of the working roller/°;
λ	- thermal diffusivity of rolling workpiece;
F	-rolling force/kN;
k_f	- deformation resistance/(MPa/kN);
σ_f	- forward tension/MPa;
σ_b	- backward tension/MPa;
R	- initial roll radius/MPa;
E	- elastic modulus/MPa;
Q_{p}	-state coefficient of stress;
F_0	- zeroing force/kN;
m_{f}	-state coefficient of entry tension;
m_{b}	- state coefficient of exit tension;
M_{m}	- mill stiffness/(kN/mm);
S_0	- roll gap without load/mm;
$v_{\mathrm{out,i}}$	-exit speed of the strip at the ith stand/(mm/s);
$v_{\mathrm{in,i+1}}$	- entry speed at the (i+1)th stand/(mm/s);
c_{f}	- viscous friction constant,
L	-distance between adjacent stands/mm;
$L(\theta)$	- actual length of the strip/mm;
V_i	-working roller speed at the ith stand/(m/s);
ϕ_n	- neutral angle/rad
L_1	-distance between the actual pass line and the looper pivot/mm;
L_2	- distance between the stand and the looper pivot/mm;
L_3	- length of the looper arm/mm;
r	- radius of the looper roll/mm;
J	-looper moment of inertia;
M	- looper motor torque/(kgm^2);

M_L - looper load torque/(kgm^2);
M_g - torque from looper roll and strip weight/(kgm^2);
W_S - strip mass;
W_R -looper roll mass.

REFERENCES

[1] Q.-K. Pan, L. Gao, and L. Wang, "A multi-objective hot-rolling scheduling problem in the compact strip production," *Appl. Math. Model.*, vol. 73, pp. 327–348, Sep. 2019.
[2] J. Pittner and M. A. Simaan, "Advanced control to reduce the likelihood of cobbles in the tandem rolling of hot metal strip," *IEEE Trans. Ind. Appl.*, vol. 51, no. 5, pp. 4305–4312, Sep./Oct. 2015.
[3] J. Dong, Z. Shi, and R. Sun, "An output probabilistic constrained optimal control algorithm based on multivariable MAC and its application in looper control system," *IEEE Access*, vol. 7, pp. 72885–72895, 2019.
[4] L. Sun, C. Shao, and L. Zhang, "Dynamic tracking prediction control of exit strip thickness based on improved fractal," *Metall. Res. Technol.*, vol. 114, no. 4, p. 412, 2017.
[5] Y. Fang-chen, S. Jie, Z. Dian-Hua, and M. Geng-sheng, "Sliding mode variable structure control for smith prediction monitoring AGC system based on double power reaching law," *J. Brazilian Soc. Mech. Sci. Eng.*, vol. 38, no. 6, pp. 1731–1743, Aug. 2016.
[6] I.-S. Choi, J. A. Rossiter, and P. J. Fleming, "Robust constrained predictive controllers for hot rolling mills: Disturbance uncertainty case," *Proc. Inst. Mech. Eng. I, J. Syst. Control Eng.*, vol. 222, no. 2, pp. 137–152, Mar. 2008.
[7] Z. Zhong and J. Wang, "Looper-tension almost disturbance decoupling control for hot strip finishing mill based on feedback linearization," *IEEE Trans. Ind. Electron.*, vol. 58, no. 8, pp. 3668–3679, Aug. 2011.
[8] C. J. Park and I. C. Hwang, "Tension control in hot strip process using adaptive receding horizon control," *J. Mater. Process. Technol.*, vol. 209, no. 1, pp. 426–434, Jan. 2009.
[9] G. Hearns and M. J. Grimble, "Robust multivariable control for hot strip mills," *ISIJ Int.*, vol. 40, no. 10, pp. 995–1002, 2000.
[10] M. Okada, K. Murayama, A. Urano, Y. Iwasaki, A. Kawano, and H. Shiomi, "Optimal control system for hot strip finishing mill," *Control Eng. Pract.*, vol. 6, no. 8, pp. 1029–1034, Aug. 1998.
[11] J. Pittner and M. A. Simaan, "Improvement in control of the tandem hot strip mill," *IEEE Trans. Ind. Appl.*, vol. 49, no. 5, pp. 1962–1970, Sep. 2013.
[12] J. Xiao-hong, L.-P. Shao, and Y. Peng, "Adaptive coordinated control for hot strip finishing mills," *J. Iron Steel Res. Int.*, vol. 18, no. 4, pp. 36–43, Apr. 2011.
[13] L. Qu, J. Wang, and S.-Y. Zong, "Decoupling control strategy for the AGC-LP system," *Iron Steel*, vol. 43, no. 10, pp. 55–58, 2008.
[14] F. A. Cuzzola, "A multivariable and multi-objective approach for the control of hot-strip mills," *J. Dyn. Syst., Meas., Control*, vol. 128, no. 4, pp. 856–868, Dec. 2006.
[15] G. Hearns, P. Smith, T. Bilkhu, and P. Reeve, "Hot strip mill multivariable mass flow control," *IEE Proc.-Control Theory Appl.*, vol. 151, no. 4, pp. 386–394, Jul. 2004.
[16] F.-C. Yin, J. Sun, W. Peng, H.-Y. Wang, J. Yang, and D.-H. Zhang, "Dynamic matrix predictive control for a hydraulic looper system in hot strip mills," *J. Central South Univ.*, vol. 24, no. 6, pp. 1369–1378, Jun. 2017.
[17] I. S. Choi, A. Rossiter, B. Pluymers, P. Fleming, and B. De Moor, "A robust MPC design for hot rolling mills: A polyhedral invariant sets approach," in *Proc. Amer. Control Conf.*, Jun. 2006, pp. 875–880.
[18] S. K. Yildiz, J. F. Forbes, B. Huang, Y. Zhang, F. Wang, V. Vaculik, and M. Dudzic, "Dynamic modelling and simulation of a hot strip finishing mill," *Appl. Math. Model.*, vol. 33, no. 7, pp. 3208–3225, Jul. 2009.
[19] S. K. Yildiz, B. Huang, and J. F. Forbes, "Dynamics and variance control of hot mill loopers," *Control Eng. Pract.*, vol. 16, no. 1, pp. 89–100, Jan. 2008.
[20] B. Ginzburg, *Steel-Rolling Technology: Theory and Practice*. New York, NY, USA: Marcel Dekker, 1989.
[21] S. K. Pal and D. A. Linkens, "Temperature distribution in steel during hot rolling: Pseudo-bond graph view," *Simul. Model. Pract. Theory*, vol. 10, nos. 1–2, pp. 69–85, Oct. 2002.
[22] J. Pian and Y. Zhu, "A hybrid soft sensor for measuring hot-rolled strip temperature in the laminar cooling process," *Neurocomputing*, vol. 169, pp. 457–465, Dec. 2015.
[23] H. Ford and J. M. Alexander, "Simplified hot-rolling calculations," *J. Inst. Met.*, vol. 192, no. 64, pp. 397–404, 1963.
[24] R. B. Sims, "The calculation of roll force and torque in hot rolling mills," *Proc. Inst. Mech. Eng.*, vol. 168, no. 1, pp. 191–200, Jun. 1954.
[25] C. Yin, H. Zhang, and C. Zhang, "Dynamic modeling and rolling data analysis of the tandem hot rolling process," *Trans. Soc. Model. Simul. Int.*, vol. 93, no. 4, pp. 307–321, 2017.
[26] H. Cai, P. Li, C. Su, and J. Cao, "Robust model predictive control for a class of discrete-time Markovian jump linear systems with operation mode disordering," *IEEE Access*, vol. 7, pp. 10415–10427, 2019.
[27] P. Sopasakis and H. Sarimveis, "Stabilising model predictive control for discrete-time fractional-order systems," *Automatica*, vol. 75, pp. 24–31, Jan. 2017.

FANGCHEN YIN received the B.S. degree in material processing engineering from the Shenyang University of Technology, in 2011, and the M.S. and Ph.D. degrees in material processing engineering from Northeastern University, Shenyang, China, in 2013 and 2017, respectively.

He is currently an Assistant Professor with Huaqiao University, Xiamen, China. His research interests include model predictive control, control system design, and control system simulation.